

Effective Hamiltonian Methods for Predicting the Electrocaloric Behavior of BaTiO₃

S. P. Beckman^{a,b,*}, L. F. Wan^a, Jordan A. Barr^a, Takeshi Nishimatsu^{a,b}

^aDepartment of Materials Science and Engineering, Iowa State University, Ames, Iowa 50011

^bInstitute for Materials Research (IMR), Tohoku University, Sendai 980-8577, Japan

Abstract

The perovskite crystal BaTiO₃ is modeled using a first-principles based effective Hamiltonian and molecular dynamics simulations are performed to estimate the pyroelectric response. The electrocaloric temperature change, ΔT , is calculated for different temperatures and externally applied electric fields. It is found that it is possible to achieve a large ΔT , around 5-6 K, for a relatively small electric field gradient, less than 100 kV/cm, if the applied fields have a small absolute magnitude.

Keywords: BaTiO₃, pyroelectric, electrocaloric effect, simulation

1. Introduction

A pyroelectric crystal develops a spontaneous electrical polarization when its temperature changes. [1] Its enthalpy can be expressed as $H = E - \mathcal{E}P$, where E is the internal energy, \mathcal{E} is an applied electric field, and P is the polarization. It is possible to cycle the temperature and electric field, to drive the crystal through an order/disorder phase transition, such as the ferroelectric/paraelectric transition in perovskite crystals, to convert between heat and electric energies. The phenomena known as the electrocaloric effect (ECE), in which electrical energy is used to induce a temperature change, is directly related to this thermodynamic cycle. The ECE is not only interesting from a fundamental science perspective, but also holds great potential for future technologies such as solid-state refrigeration.

The ECE was first discovered in 1930 [2], but there were few studies pursued until ferroelectric crystals, with permanent dipoles, were discovered. The initial studies focused on bulk ceramics including Rochelle salt [3], SrTiO₃ [4], BaTiO₃ (BTO) [5], and doped alkali halides [6, 7, 8]; however, the engineering potential of these crystals was never realized.

In 2006 Mischenko *et al.* discovered the “giant electrocaloric effect” in Zr-rich PbZr_{0.95}Ti_{0.05}O₃ (PZT) thin films. [9] By using a thin film it was possible to apply ultra-high electric fields, to achieve an ECE ΔT of 12 K. The discovery of the giant ECE has revitalized the field and has inspired numerous recent studies investigating the impact of ultra-high electric fields on the pyroelectric response of other ferroelectric materials.

The initial work focused on Zr-rich PZT, [9] and although this alloy is still being investigated, [10, 11] there has also been a great deal of interest in other perovskite crystals including $(1-x)\text{PbMg}_{1/3}\text{Nb}_{2/3}\text{O}_3$ - $x\text{PbTiO}_3$ [12, 13], BTO [14, 15, 16, 17, 18, 19], BaTiO₃-SrTiO₃ superlattices [20], and SrBi₂Ta₂O₉ layered oxides [21]. In addition there has been much interest in the development of polymer based ferroelectrics, such as poly(vinylidene fluoride-trifluoroethylene) and poly(vinylidene fluoride-trifluoroethylene-chlorofluoroethylene). [22, 23]

In this paper we will focus on the BTO compound for a variety of reasons: it is a well studied archetypical perovskite crystal that is relatively easy to produce, it exhibits an excellent pyroelectric response, it does not contain the toxin lead, its ferroelectric properties have the potential to be tailored by alloying or the creation of superlattice structures. The ECE in BTO has been previously

*Corresponding author

Email address: sbeckman@iastate.edu (S. P. Beckman)

studied as a thin film[14, 15] and as a thick film in a multi-layer stack. [16, 17] Surprisingly, off-the-shelf BTO multilayer capacitors have been shown to exhibit a reasonable electrocaloric response. [18] There also has been a study of the properties of BTO nanoparticles with core-shell geometries. [19]

Previous theoretical studies of BTO have largely relied on thermodynamic models, for example the Ginzburg-Landau-Devonshire model. [15, 16, 17, 19, 20, 11] While these have proven successful, they require a large amount of data to accurately parameterize the model. One alternative approach was demonstrated by Cao and Li in which they created a transverse Ising model (TIM) to study the ECE in BTO thin-films. They predict that compressive epitaxial strains result in increasing the temperature where the ECE is maximum and tensile strains reduce the temperature. [14] The TIM model is particularly interesting because in addition to the spin exchange interactions, taken up to four spins, the effect of quantum fluctuations were also included. It is reported that increasing the strength of the quantum fluctuations results in shifting the ECE to higher temperatures. Bellaiche *et al.* have used a molecular dynamics approach to investigate nanodots of $\text{Pb}(\text{Zr}_{0.4}\text{Ti}_{0.6})\text{O}_3$. They report the time dependency of the temperature when an alternating electric field is applied. [10] It is discovered that it may be possible to tune the ECE in nanodots by adjusting the depolarization field, which in practical terms would be implemented by modifying the surface of the nanodot.

Following this introduction the theoretical methods are presented. The results are presented and discussed in section 3. The manuscript concludes with a summary in section 4.

2. Methods

Here we predict the ECE for BTO using the model Hamiltonian,

$$\begin{aligned}
H^{\text{eff}} = & \frac{M_{\text{dipole}}^*}{2} \sum_{\mathbf{R}, \alpha} \dot{u}_{\alpha}^2(\mathbf{R}) + \frac{M_{\text{acoustic}}^*}{2} \sum_{\mathbf{R}, \alpha} \dot{w}_{\alpha}^2(\mathbf{R}) \\
& + V^{\text{self}}(\{\mathbf{u}\}) + V^{\text{dpl}}(\{\mathbf{u}\}) + V^{\text{short}}(\{\mathbf{u}\}) \\
& + V^{\text{elas, homo}}(\eta_1, \dots, \eta_6) + V^{\text{elas, inho}}(\{\mathbf{w}\}) \\
& + V^{\text{coup, homo}}(\{\mathbf{u}\}, \eta_1, \dots, \eta_6) + V^{\text{coup, inho}}(\{\mathbf{u}\}, \{\mathbf{w}\}) \\
& - Z^* \sum_{\mathbf{R}} \mathcal{E} \cdot \mathbf{u}(\mathbf{R}), \quad (1)
\end{aligned}$$

which is derived in Refs. [24, 25]. The true atomic structure has properties that are determined by the complex chemical bonding between the atoms, but in the model system the complexity is reduced; the collective atomic motion is coarse-grained by local softmode vectors $\mathbf{u}(\mathbf{R})$ and local acoustic displacement vectors $\mathbf{w}(\mathbf{R})$ of each unit cell at \mathbf{R} in a simulation supercell as well as the homogeneous strain components, $(\eta_1, \eta_2, \eta_3, \eta_4, \eta_5, \eta_6)$. The terms in the Hamiltonian bear a physical significance: $\frac{M_{\text{dipole}}^*}{2} \sum_{\mathbf{R}, \alpha} \dot{u}_{\alpha}^2(\mathbf{R})$ and $\frac{M_{\text{acoustic}}^*}{2} \sum_{\mathbf{R}, \alpha} \dot{w}_{\alpha}^2(\mathbf{R})$ is the kinetic energy possessed by the local soft modes and the local acoustic displacement vectors, $V^{\text{self}}(\{\mathbf{u}\})$ is the local mode self energy, $V^{\text{dpl}}(\{\mathbf{u}\})$ is the long-ranged dipole-dipole interaction, $V^{\text{short}}(\{\mathbf{u}\})$ is the short-ranged interaction between local soft modes, $V^{\text{elas, homo}}(\eta_1, \dots, \eta_6)$ is the elastic energy from homogeneous strains, $V^{\text{elas, inho}}(\{\mathbf{w}\})$ is the elastic energy from inhomogeneous strains, $V^{\text{coup, homo}}(\{\mathbf{u}\}, \eta_1, \dots, \eta_6)$ is the coupling between the local soft modes and the homogeneous strain, $V^{\text{coup, inho}}(\{\mathbf{u}\}, \{\mathbf{w}\})$ is the coupling between the soft modes and the inhomogeneous strains, and $-Z^* \sum_{\mathbf{R}} \mathcal{E} \cdot \mathbf{u}(\mathbf{R})$ is the electric enthalpy. Each of the terms in Eq.1 is expanded to allow the Hamiltonian to be expressed using the parameterization given in Refs. [24, 25, 26, 27, 28]. The same set of parameters in Ref. [28] for BaTiO_3 is used in this letter. Values of the 25 parameter are also given as Supplementary Data to this letter. The details of the molecular dynamics method are explained in Refs. [26, 27]. The method described here is encoded in the software package **feram**, which is distributed freely to the scientific community.¹

The simulation uses a supercell of size $N = L_x \times L_y \times L_z = 16 \times 16 \times 16$ and the temperature is scanned from 250 K to 900 K at an increment of +1 K/step. For each temperature increment, the system is thermalized for 20,000 time steps, after which the properties are averaged for 80,000 time steps, using a time step of $\Delta t = 2$ fs. The simulations begin at low temperature with a z -polarized initial configuration that is random. As described in Ref. [28], thermal expansion is simulated by including a temperature-dependent effective negative pressure $p = -0.005T$ GPa. It has been shown in Ref. [28] that the parameterization

¹The MD code “**feram**” can be downloaded from <http://loto.sourceforge.net/feram/> as free software.

used here offers an improved estimation of ferroelectric (tetragonal) to paraelectric (cubic) transition temperature and c/a ratio as compared to earlier models [24, 25]. Therefore, we believe that this set of parameters also gives a good estimation of the pyroelectric properties.

The complex interactions, such as the interaction of domain walls with crystal defects and interfaces that are present in experimental systems are not present here. This makes direct comparison between computational and experimental results challenging; however, these calculations are intended to isolate the essential physics of the crystal and the pyroelectric response due to the bonds between the metal cations and the oxygen. It is anticipated that the fundamental behavior observed in these calculations will also be present in the experimental systems. In principle the predicted ECE response will be observed in high purity single crystals of BTO, although such experimental systems are challenging to prepare.

3. Results and Discussion

Simulations are performed for constant electric fields ranging from 25 to 310 kV/cm at an increment of 5 kV/cm. This temperature range focuses on the ferroelectric (tetragonal) to paraelectric (cubic) transitions, where the largest pyroelectric response should be observed. The z -component of polarization, P_z , is calculated from the MD simulation results and is plotted versus T at constant \mathcal{E}_z in Fig. 1(a). The data are fitted with weighted splines to allow for the determination of $\partial P_z / \partial T$, which is shown in Fig. 1(b) and Fig. 2. Cooling-down simulations are also performed and hysteresis in temperature is found when $\mathcal{E}_z \leq 25$ kV/cm, as seen in the $\mathcal{E}_z = 0$ kV/cm simulations in Fig. 1(a). In the simulations, the phase-transition order changes from first to second around $\mathcal{E}_z = 25$ kV/cm. To focus our theoretical effort on the determination of the pyroelectric response without including the additional complexity of the latent heat of transformation, only fields $\mathcal{E}_z \geq 60$ kV/cm are used in the present calculations.

Following Ref. [9], the electrocaloric refrigeration ΔT is estimated using

$$\Delta T = \frac{-1}{C_v} \int_{\mathcal{E}_1}^{\mathcal{E}_2} T \frac{\partial P_z}{\partial T} d\mathcal{E}_z \quad (2)$$

as shown in Fig. 3. For heat capacity, experimental, temperature and electric-field independent

value of $C_v = 5.84 \text{ g} \cdot \text{cm}^{-3} \times 0.434 \text{ J} \cdot \text{g}^{-1} \cdot \text{K}^{-1}$ or $2.53 \text{ J} \cdot \text{cm}^{-3} \cdot \text{K}^{-1}$ is used in this estimation [29]; the coarse-graining used in the effective Hamiltonian method makes it difficult to correctly estimate the heat capacity. The integral in Eqn. 2 ranges over $\Delta \mathcal{E} = \mathcal{E}_2 - \mathcal{E}_1$. The fields used for this integral are specified in the legends of Fig. 3 as, “ $\mathcal{E}_1 \dots \mathcal{E}_2$.”

Because the phase transition becomes increasingly diffuse as the electric field is increased the greatest pyroelectric response, $\partial P_z / \partial T$ shown in Fig. 1 (b), occurs at lower electric fields. In Fig. 3 frame (a) the field gradient $\Delta \mathcal{E}$ is varied and \mathcal{E}_2 is held constant at 310 kV/cm. The magnitude of the ECE ΔT is proportional to the magnitude of the field gradient, $\Delta \mathcal{E}$. This is entirely consistent with the experimental observations. The temperature where the maximum ΔT occurs is determined by the isothermal curve in Fig. 1 that makes the greatest contribution within the field range bracketed by \mathcal{E}_1 and \mathcal{E}_2 . For example, over the range $\mathcal{E}_1 = 160$ and $\mathcal{E}_2 = 310$ kV/cm the $T = 550.5$ and 600.5 K curves have the greatest magnitude in Fig. 2 and the ΔT versus T curve, in Fig. 3 (a), peaks just above $T = 550$ K.

It is observed by Akcay *et al.* that not only is the field gradient, $\Delta \mathcal{E}$, important but also the absolute magnitude of the fields \mathcal{E}_1 and \mathcal{E}_2 . In Fig. 3 (b) the field gradient is held constant at $\Delta \mathcal{E} = 100$ and \mathcal{E}_1 is varied from 60 to 210 kV/cm. At larger absolute fields the diffuse nature of the phase transition results in a decrease in the magnitude of the ECE ΔT as well as an increase in the temperature where ΔT is maximum. As a matter of practice this means that the ECE will always occur above the Curie temperature. Comparing the results in Fig. 3 (a) and (b) it is observed that by keeping \mathcal{E}_1 small it is possible to achieve large ΔT for small $\Delta \mathcal{E}$, and when \mathcal{E}_1 becomes large it is necessary to have a large $\Delta \mathcal{E}$ to have comparable ΔT . The implication of this observation is that compounds with antiferroelectric ordering, which require large \mathcal{E}_1 , [9] may not be the optimal choice for producing a large ECE.

4. Summary

In summary, we have demonstrated the use of our MD method **feram** to estimate the ECE as functions of temperature and external fields. The freely available method used here can be parameterized using first-principles results alone, and therefore can be extended to investigate systems that lack

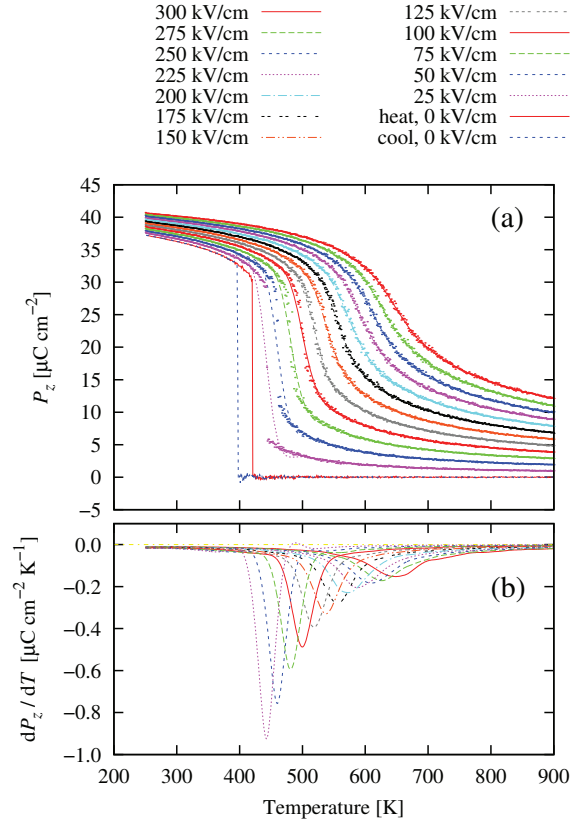


Figure 1: (color online) The calculated pyroelectric response. (a) The simulated temperature dependence of the polarization along the z -direction at constant external electric field is determined. The simulated data is plotted as dots and are fitted using weighted splines, shown as lines. $\mathcal{E}_z = 0$ kV/cm heating-up and cooling-down results are also plotted for reference. (b) The pyroelectric coefficient, $\partial P_z / \partial T$, is determined from the fitted data.

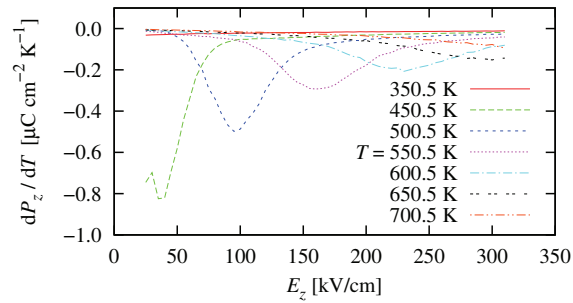


Figure 2: (color online) The pyroelectric coefficient, $\partial P_z / \partial T$, is determined as a function of electric field at constant temperature from the fitted data in Fig. 1.

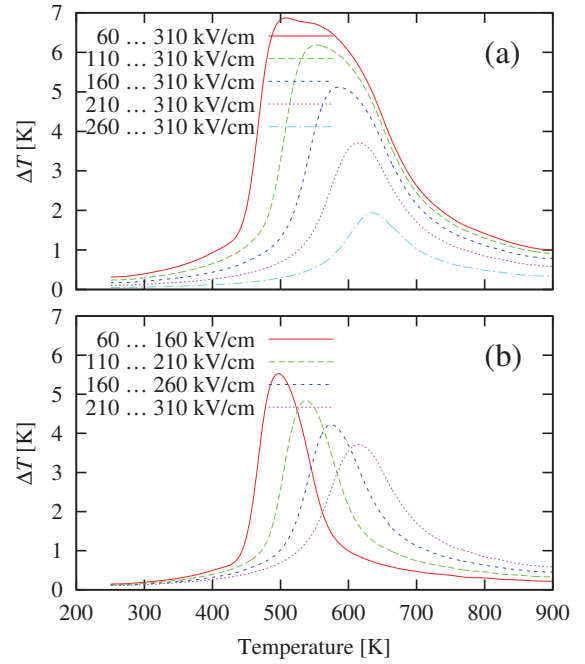


Figure 3: (color online) The predicted electrocaloric effect estimated from Eqn. 2. The integral range $\mathcal{E}_1 \dots \mathcal{E}_2$ is specified in the plot legend. (a) The value of \mathcal{E}_2 is held fixed at 310 kV/cm and \mathcal{E}_1 is varied to give the $\Delta\mathcal{E}$ the values 250, 200, 150, 100, and 50 kV/cm. (b) The values of \mathcal{E}_1 and \mathcal{E}_2 are changed together to maintain a fixed value of $\Delta\mathcal{E} = 100$ kV/cm.

sufficient experimental data to produce an accurate thermodynamical model. We have demonstrated the effect of varying electric fields on the archetypical pyroelectric, BTO, and have found that to produce a large ECE for a relatively small field gradient, it is preferred to not have an antiferroelectric ground state, which will allow the use of modest fields. While admittedly the external electric fields consider here may be slightly high compared to the breakdown voltage of polycrystalline BaTiO₃; advancements in synthesis techniques, such as vapor deposition processes, hold the promise of creating affordable high quality ferroelectric thin films that can withstand these electric fields.

5. Acknowledgements

The work of SPB, JAB, and LFW was supported by the National Science Foundation (NSF) through Grant DMR-1037898 and DMR-1105641. SPB would like to thank the International Collaboration Center at the Tohoku University Institute for Materials Research for their support summer 2011. The work of TN was supported by Japan Society for the Promotion of Science (JSPS) through KAKENHI 23740230. Computational resources were provided by the Center for Computational Materials Science, Institute for Materials Research (CCMS-IMR), Tohoku University.

References

- [1] M. Lines, A. Glass, Principles and Applications of Ferroelectrics and Related Materials, Clarendon Press, Oxford, 1977.
- [2] P. Kobeko, I. Kurchatov, Dielectric characteristics of seignette's salts, *Z. Phys.* 66 (1930) 192–205.
- [3] G. Wiseman, J. Kuebler, Electrocaloric effect in ferroelectric rochelle salt, *Phys. Rev.* 131 (1963) 2023–2027.
- [4] E. Hegenbarth, Studies of the electrocaloric effect of ferroelectricceramics at low temperatures, *Cryogenics* 1 (1961) 242–243.
- [5] W. Lawless, Recent topics in ferroelectric properties at low temperatures, *Ferroelectrics* 24 (1980) 327–335.
- [6] W. Kanzig, J. H.R. Hart, S. Roberts, Paraelectricity and ferroelectricity due to hydroxyl ions in alkali halides; paraelectric cooling, *Phys. Rev. Lett.* 13 (1964) 543–545.
- [7] I. Shepherd, G. Feher, Cooling by adiabatic depolarization of OH[−] molecules in KCl, *Phys. Rev. Lett.* 15 (1965) 194–198.
- [8] U. Kuhn, F. Luty, Paraelectric heating and cooling with OH[−]-dipoles in alkali halides, *Solid State Commun.* 3 (1965) 31–33.
- [9] A. Mischenko, Q. Zhang, J. Scott, R. Whatmore, N. Mathur, Giant electrocaloric effect in thin-film PbZr_{0.95}Ti_{0.05}O₃, *Science* 311 (2006) 1270–1271.

- [10] S. Prosandeev, I. Ponomareva, L. Bellaiche, Electrocaloric effect in bulk and low-dimensional ferroelectrics from first principles, *Phys. Rev. B* 78 (2008).
- [11] J. Karthik, L. W. Martin, Pyroelectric properties of polydomain epitaxial pb(zr(1-x), ti(x))o(3) thin films, *Phys. Rev. B* 84 (2011).
- [12] A. Mischenko, Q. Zhang, R. Whatmore, J. Scott, N. Mathur, Giant electrocaloric effect in the thin film relaxor ferroelectric 0.9 PbMg_{1/3}Nb_{2/3}O₃-0.1 PbTiO₃ near room temperature, *Appl. Phys. Lett.* 89 (2006).
- [13] J. Hagberg, A. Uusimaki, H. Jantunen, Electrocaloric characteristics in reactive sintered 0.87 pb(mg(1/3)nb(2/3))o(3)-0.13 pbtio(3), *Appl. Phys. Lett.* 92 (2008).
- [14] H. Cao, Z. Li, Electrocaloric effect in BaTiO₃ thin films, *J. Appl. Phys.* 106 (2009).
- [15] G. Akcay, S. Alpay, J. Mantese, G. Rossetti, Magnitude of the intrinsic electrocaloric effect in ferroelectric perovskite thin films at high electric fields, *Appl. Phys. Lett.* 90 (2007).
- [16] Y. Bai, G. Zheng, S. Shi, Kinetic electrocaloric effect and giant net cooling of lead-free ferroelectric refrigerants, *J. Appl. Phys.* 108 (2010).
- [17] Y. Bai, G. Zheng, S. Shi, Kinetic electrocaloric effect and giant net cooling of lead-free ferroelectric refrigerants, *J. Appl. Phys.* 96 (2010).
- [18] S. Kar-Narayan, N. D. Mathur, Direct and indirect electrocaloric measurements using multilayer capacitors, *J. Phys. D Appl. Phys.* 43 (2010).
- [19] C. Fang, D. Zhou, S. Gong, Core-shell structure and size effect in barium titanate nanoparticle, *Physica B* 406 (2011) 1317–1322.
- [20] J. H. Qiu, Q. Jiang, Orientation dependence of the electrocaloric effect of ferroelectric bilayer thin films, *Solid State Commun.* 149 (2009) 1549–1552.
- [21] H. Chen, T.-L. Ren, X.-M. Wu, Y. Yang, L.-T. Liu, Giant electrocaloric effect in lead-free thin film of strontium bismuth tantalite, *Appl. Phys. Lett.* 94 (2009).
- [22] B. Neese, B. Chu, S.-G. Lu, Y. Wang, E. Furman, Q. M. Zhang, Large electrocaloric effect in ferroelectric polymers near room temperature, *Science* 321 (2008) 821–823.
- [23] S.-G. Lu, Q. Zhang, Electrocaloric materials for solid-state refrigeration, *Adv. Mater.* 21 (2009) 1983–1987.
- [24] R. D. King-Smith, D. Vanderbilt, First-principles investigation of ferroelectricity in perovskite compounds, *Phys. Rev. B* 49 (1994) 5828–5844.
- [25] W. Zhong, D. Vanderbilt, K. M. Rabe, First-principles theory of ferroelectric phase-transitions for perovskites - the case of batio₃, *Phys. Rev. B* 52 (1995) 6301–6312.
- [26] T. Nishimatsu, U. V. Waghmare, Y. Kawazoe, D. Vanderbilt, *Phys. Rev. B* 78 (2008) 104104.
- [27] U. V. Waghmare, E. J. Cockayne, B. P. Burton, Ferroelectric phase transitions in nano-scale chemically ordered pb_{0.5}nb_{0.5}o₃ using a first-principles model hamiltonian, *Ferroelectrics* 291 (2003) 187–196.
- [28] T. Nishimatsu, M. Iwamoto, Y. Kawazoe, U. V. Waghmare, First-principles accurate total energy surfaces for polar structural distortions of batio₃, pbtio₃, and srtio₃: Consequences for structural transition temperatures, *Phys. Rev. B* 82 (2010) 134106.
- [29] Y. He, Heat capacity, thermal conductivity, and thermal expansion of barium titanate-based ceramics, *Thermochimica Acta* 419 (2004) 135 – 141.